Nano Energy 35 (2017) 387–395

Contents lists available at ScienceDirect

Nano Energy

journal homepage: www.elsevier.com/locate/nanoen

Full paper

Record high thermoelectric performance in bulk $SrTiO_3$ via nano-scale modulation doping

Jun Wang[a,h,*,1], Bo-Yu Zhang[a], Hui-Jun Kang[b,1], Yan Li[a], Xinba Yaer[a,h], Jing-Feng Li[c], Qing Tan[c], Shuai Zhang[d], Guo-Hua Fan[e], Cheng-Yan Liu[f], Lei Miao[f], Ding Nan[a,h], Tong-Min Wang[b,**], Li-Dong Zhao[g,**]

[a] School of Materials Science and Engineering, Inner Mongolia University of Technology, No. 49 Ai Min Road, Xin Cheng Qu, Hohhot, Inner Mongolia Autonomous Region 010051, China
[b] Key Laboratory of Solidification Control and Digital Preparation Technology (Liaoning Province), School of Materials Science and Engineering, Dalian University of Technology, Dalian 116024, China
[c] State Key Laboratory of New Ceramics and Fine Processing, School of Materials Science and Engineering, Tsinghua University, Beijing 100084, China
[d] Beijing National Laboratory for Condensed Matter Physics, and Institute of Physics, Chinese Academy of Sciences, Beijing 100190, China
[e] School of Materials Science and Engineering, Harbin Institute of Technology, Harbin 150001, China
[f] Guangxi Key Laboratory of Information Material, Guangxi Collaborative Innovation Center of Structure and Property for New Energy and Materials, School of Material Science and Engineering, Guilin University of Electronic Technology, Guilin 541004, China
[g] School of Materials Science and Engineering, Beihang University, Beijing 100191, China
[h] Inner Mongolia Key Laboratory of Thin Film and Coatings Technology, No. 49 Ai Min Road, Xin Cheng Qu, Hohhot, Inner Mongolia Autonomous Region 010051, China

ARTICLE INFO

Keywords:
Thermoelectric materials
Strontium titanate
Cold isostatic pressing
Microstructure
Effective mass

ABSTRACT

Strontium titanite ($SrTiO_3$), which is an experimentally-friendly thermoelectric material, could be a promising candidate for thermoelectric power generation applications. The theorectical study indicates the co-doping of La and Nb could enhance the thermoelectric performance, however, the thermoelectric figure of merits (*ZT*s) of $SrTiO_3$ are still low because the co-doping process at nano-scale is experimentally difficult to control. Here we report a high performance $SrTiO_3$ with La-Nb co-doping, which are prepared by a combination of hydrothermal method and high-efficiency sintering. Nano-scale co-doping is successfully modulated by hydrothermal method, and nano-inclusions precipitate during sintering process, to form complex microstructures. In this case, the electrical and thermal transport properties are optimized simultaneously by doping concentration and dopants type, resulting in a record-high $ZT > 0.6$ at 1000–1100 K in the 10 mol% La and 10 mol% Nb doped $SrTiO_3$ bulk materials. The nano-scale modulation doping and microstructure controlling approach validated in the present study should be also applicable for other thermoelectric materials.

1. Introduction

Thermoelectric devices can directly convert heat to electrical energy, which benefits to the improvement of energy efficiency, and reduces environmental pollution. The efficiency of a thermoelectric device is determined by the thermoelectric dimensionless figure of merit, $ZT = S^2\sigma T/\kappa$, where S, σ, κ and T are the Seebeck coefficient, electrical conductivity, thermal conductivity and working temperature in Kelvin, respectively. Fine tuning of two interdependent transport parameters simultaneously, e.g. improvement of electronic transport and decreasing of thermal transport are crucial for obtaining a high *ZT* value. Several experimental methods and mechanisms have been introduced to increase the *ZT* of alloy thermoelectric materials [1–5]. Appreciably high *ZT* values have also been obtained from some non-metal thermoelectric materials by effectively modulating microstructure design [6–9]. However, the *ZT* values of n-type oxide bulk materials are still low [10–12] compared to that of the alloys and the p-type oxides [13,14].

$SrTiO_3$ is a typical perovskite oxide n-type thermoelectric material with the potential for the high temperature thermoelectric applications because of its special merits such as high chemical and thermal stability, environmental compatibility and low toxicity. However, from

* Correspondence to: School of Materials Science and Engineering, Inner Mongolia University of Technology, Hohhot, Inner Mongolia, 010051,China.
** Corresponding authors.
E-mail addresses: wangjun@imut.edu.cn (J. Wang), tmwang@dlut.edu.cn (T.-M. Wang), zhaolidong@buaa.edu.cn (L.-D. Zhao).
[1] These authors contributed equally to this work.

http://dx.doi.org/10.1016/j.nanoen.2017.04.003
Received 22 January 2017; Received in revised form 26 March 2017; Accepted 3 April 2017
Available online 06 April 2017

the first report on thermoelectric performance examined in $SrTiO_3$ bulk materials in 1964 [15], the *ZT* values have never exceeded 0.4 [12]. Previous experimental results show that the *ZT* value can be remarkably improved upon doping La or Nb in $SrTiO_3$ (*ZT*=0.3–0.4) [12,16,17]. On the other hand, a theorectical study [18] also predicted that the co-doping of La and Nb could enhance the thermoelectric performance (*ZT*=0.7) by promoting respective contributions of two element in nanostructure, motivating lots of experimental studies on this approach. However, the obtained *ZT* value of La and Nb co-doped ceramics is as small as < 0.3 at 473 K [19], which is far from the expected value in the theorectical study [18]. One possible reason is that the solid-state reaction method used in the co-doping process hardly modulates the doping in nano-scale. To introduce the nanostructure, strategies such as addition of nano-sized second phase have been introduced to improve electrical conductivity and to reduce the thermal conductivity [20,21]. However the Seebeck coefficient is relatively small in this case because the second phase has not impacted on electron structure of matrix, which not results in *ZT* value (< 0.4) improvement significantly. Thus, microstructure and electron structure controlling by nano-scale modulation doping approach is expected to realize a high thermoelectric performance in $SrTiO_3$ ceramics. The hydrothermal method, which has been successfully used in several thermoelectric materials, is suitable to synthesize high quality nanopowder [16]. To the best of our knowledge, however, to date there is no report about the hydrothermal synthesizing of La and Nb co-doped $SrTiO_3$ powders.

On the other hand, the high-cost and low preparation efficiency of conventional sintering methods for oxide materials such as spark plasma sintering [16,22], hot pressing [23] and microstructure anisotropy [22] of their products are the key reason for the limited improvement of oxide thermoelectric materials and further commercial use of these materials [24]. Thus, a practical preparation method, which is effective on controlling of microstructure and simultaneously optimizing both electronic and thermal transport properties of $SrTiO_3$ bulk materials, is imperative.

In this work, we introduced a promising preparation method which is a combination of hydrothermal method and high-efficiency sintering method, as shown in Fig. 1. Nano powders with different doping concentrations of Nb and La were successfully synthesized by the hydrothermal method (HTS), and then the powders were compacted into a disk by die pressing followed by cold isostatic pressing (CIP). After that, the disk samples were embedded by carbon powders and sintered in a muffle furnace. This approach not only can prepare large amounts of bulk samples, but also is free from some hazardous gases such as H_2 and CO in annealing process [12,25,26]. Importantly, the second phases and nano-inclusions are precipitated from the co-doped matrix to form a unique microstructure which is different from nanostructuring [16] and nano-sized composite [20]. The present microstructures effectively enhance Seebeck coefficient and decreases thermal conductivity, resulting in a record-high *ZT* > 0.6 at 1000–1100 K in $SrTiO_3$ bulk materials.

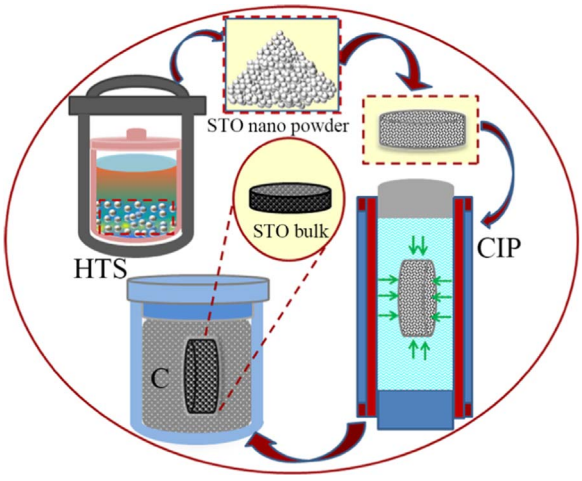

Fig. 1. Schematic diagram of preparation method, CIP: cold isostatic pressing, HTS: hydrothermal synthesis.

2. Material and methods

2.1. Sample preparation

10–30 mol% Nb and La single or co-doped $SrTiO_3$ nano powders were prepared by a hydrothermal method using Teflon lined stainless-steel autoclave containing mixture solution of $Ti(OBu)_4$, $Sr(NO_3)_2$, NaOH, ethylene glycol, $La(NO_3)_3$ and $NbCl_5$, which was heated at 180 °C for 24 h. The obtained powders were pressed by cold isostatic pressing under 250 MPa after preshaping into disk under 4 MPa. The disk samples were then embedded into carbon powders placed in a corundum crucible and sintered at 1573 K for 5 h in a muffle furnace. After sintering, the disk sample is polished sufficiently to remove the carbon on surface.

2.2. Sample characterization

All the specimens were characterized by the scanning electron microscope (SEM, FEI Quanta FEG-650 and JEOL JSM-7610F), X-ray diffraction (XRD, Rigaku D/Max-2500), transmission electron microscope (TEM, Tecnai G^2 F30) and scanning transmission electron microscope (STEM, Talos F200x) respectively. Electrical conductivity and Seebeck coefficient were measured from 300 to 1100 K in a helium atmosphere using a Linseis LSR-3. Thermal conductivity (κ) was calculated by equation $\kappa = DC_P\rho$, where thermal diffusivity *D* was measured by the laser flash method using Netzsch LFA 457, the specific heat C_P was measured by differential scanning calorimeter using Netzsch DSC STA 449F3 (Fig. S1) and the density ρ is measured by the Archimedes method (Table S1). The Hall coefficients were measured using the Van der Pauw technique under a reversible magnetic field of 1.5 T.

3. Results and discussion

The designing strategy for improving the thermoelectric performance of $SrTiO_3$ is described below as several rational successive steps. First, we designed a special synthesis method to fabricate the $SrTiO_3$ bulks; Second, the electrical transport properties of $SrTiO_3$ were optimized through electron doping; Third, the thermal conductivity was decreased by controlling microstructure.

By optimizing the doping concentration of Nb and La simultaneously, record high *ZT* ($0.6 \leq ZT < 0.7$) at 1000–1100 K, which is 40% higher than the highest *ZT* of 0.4 reported in the literature [12], have been achieved in $SrTiO_3$ bulks through co-doping with 10 mol% La and 10 mol% Nb (La10Nb10), as shown in Fig. 2a.

In addition to La10Nb10 sample, the samples with doping concentration of 5 mol% La –10 mol% Nb (La5Nb10) and 10 mol% La –5 mol% Nb (La10Nb5) also show high *ZT* values of $0.4 < ZT < 0.6$ at 1000–1100 K, respectively, which are also higher than the highest *ZT* (0.4) reported previously for single-doped $SrTiO_3$ bulk materials [12]. The single-doped samples such as 10 mol% Nb (Nb10) or 10 mol% La (La10) studied in this work show *ZT* values of $0.3 < ZT < 0.5$ at 1000–1100 K, respectively, which are comparable to the results reported previously [16,17,22]. However, the highest *ZT* value does not occur in 10 mol% La –20 mol% Nb (La10Nb20) co-doped sample with the highest σ (Fig. 2b) and the lowest $|S|$ (Fig. 2c), or 5 mol% La –5 mol% Nb (La5Nb5) co-doped sample with the lowest σ and the highest $|S|$. This experimental result suggests that a unique balance point of doped-materials is essential to achieve a higher value of the power factor, *PF* =

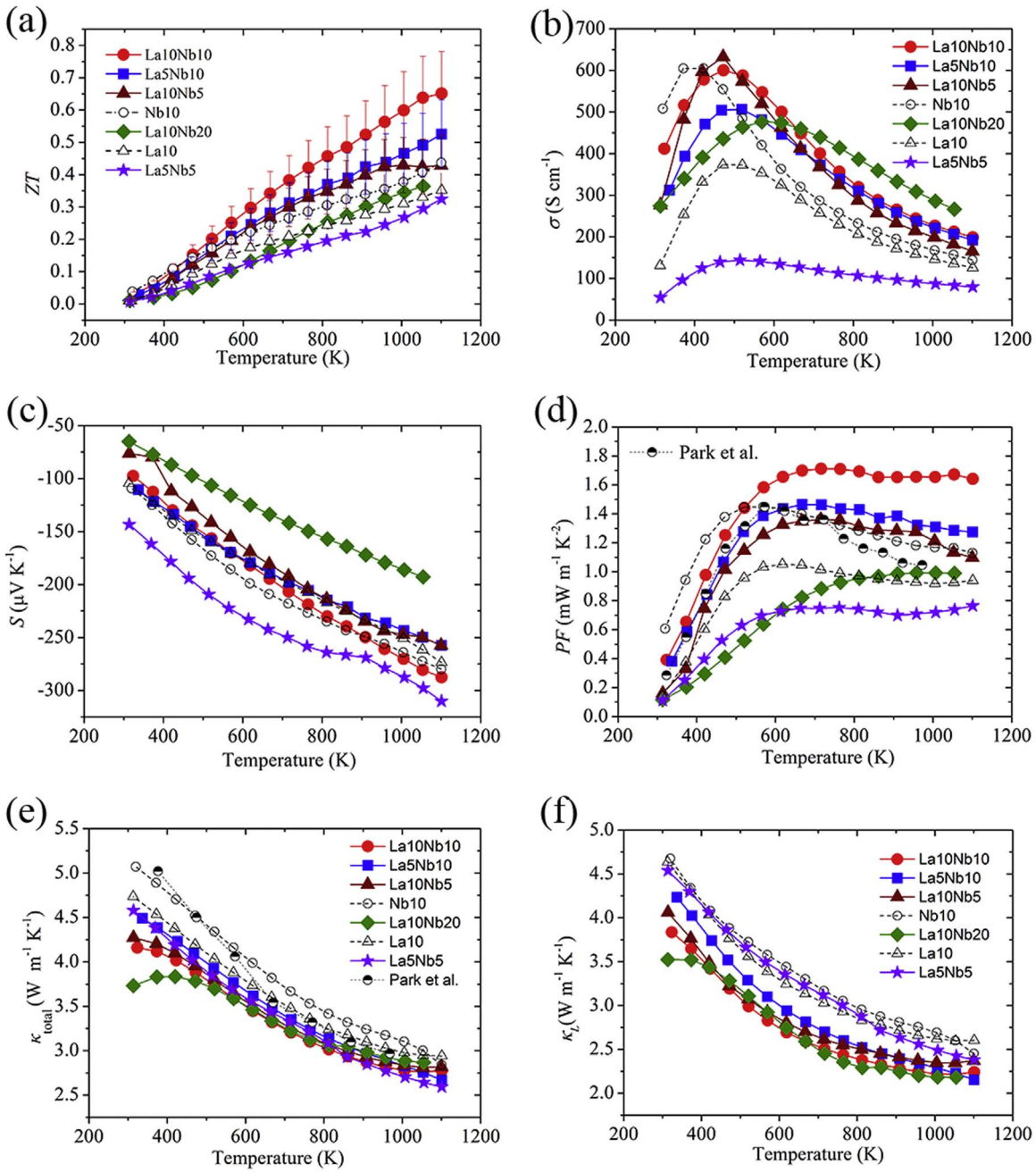

Fig. 2. Temperature dependence of (a) *ZT* values, (b) electrical conductivity (σ), (c) Seebeck coefficient (S), (d) power factor (*PF*), (e) total thermal conductivity (κ_{total}) and (f) lattice thermal conductivity κ_L.

$\sigma^2 S$ (Fig. 2d). The increase of *ZT* values obtained in this work stems from the facts of the higher *PFs* and lower thermal conductivities (Fig. 2e) as discussed in the following section.

3.1. Electrical transport properties

The electrical and thermal transport properties were measured from 300 K to 1100 K. The obvious component dependences indicate that the doping concentration, type of dopants and ratio between different dopants act differently on *S*, σ and κ (Fig. 2). The σ for samples with total doping concentrations ranging from 10 to 30 mol% displays a peak behavior between 400 and 650 K, implying a semiconductor-like mechanism as reported previously (Fig. 2b) [16,27]. Above ~650 K, the similar tendency observed in σ with different doping concentrations prompts us to discuss the doping effect on σ. The σ increases monotonically with the increase of doping concentration, suggesting that the carrier concentration is proportionally affected by changing the doping concentration ($\sigma = en\mu$, where e is the electron charge, n is the election concentration and μ is the carrier mobility). To confirm this, the Hall coefficients were measured between 300 K and 800 K. Extremely high carrier concentration of La10Nb20 leads to a Hall voltage that is too small to be measured accurately. Carrier concentrations of other co-doped sample are in the same order with nominal doping concentration and essentially constant over the measured temperature range (Fig. 3a). However, a difference of σ is found between samples with the same total nominal doping level. For example, Nb10, La10 and La5Nb5 samples show the same nominal total doping level of 10%. The former two single-doped samples have a comparable σ over a wide temperature range, whereas the latter co-doped one shows a rather small σ. Another slightly difference is also

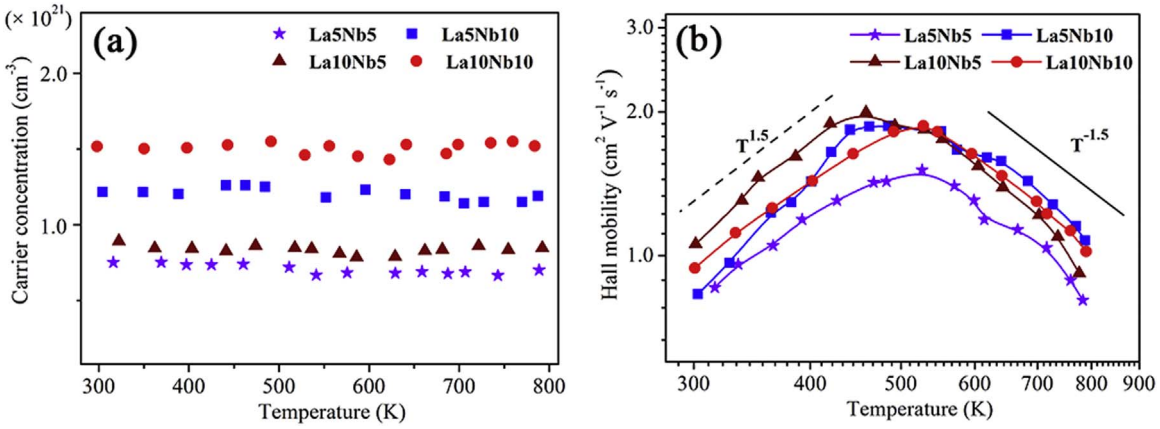

Fig. 3. Temperature dependences of carrier (a) concentration and (b) mobility of Nb and La co-doped $SrTiO_3$ bulk samples.

Table 1
Carrier effective mass (m^*/m_0), $m^*/m_0n^{2/3}$, and weighed mobility $\mu(m^*/m_0)^{3/2}$ of co-doped samples at 710 K.

La: Nb (mol%)	m^*/m_0	$m^*/(m_0n^{2/3})$ (10^{-14})	$\mu\ (m^*/m)^{3/2}$
5:5	8.8	11.2	27.1
5:10	8.0	7.1	30.5
10:5	6.6	7.5	20.2
10:10	9.8	7.5	37.4

found in the two co-doped samples with total doping concentration of 15 mol%. These phenomena are attributed to actual doping concentration (Fig. 3a) which is different from nominal doping concentration due to the precipitation of second phase (TiO_2 as observed in XRD, Fig. S2) in sintering process. In order to discuss the temperature dependence of electrical conductivity, we have showed the carrier mobility (μ) in Fig. 3b. At low temperature, the carrier mobility increases proportionally to $T^{1.5}$, indicating a developed contribution from ionized impurity scattering. The decreases of μ with proportion to $T^{-1.5}$ at high temperatures, implies a dominant scattering by acoustic phonons [28].

As shown in Fig. 2c, the S exhibits negative values in the whole temperature range, suggesting that all samples are n-type. The absolute value $|S|$ increases gradually with increasing temperature from 300 K to 1100 K, which is in good agreement with the reported results [17]. The linear temperature dependence of Seebeck coefficient is normal and suggests that the carrier concentration is constant, which in agreement with the Hall-effect measurements discussed above. The S values of La5Nb10 La10Nb5 La10Nb10 samples exceed 200 μV/K at high temperatures in spite of its high carrier concentration, which agreed well with the reported data [29]. Some previous works suggested that the heavy effective mass of carriers caused by high density of states (DOS) [24,30], high Nb concentration and large unit cell volume [17], as one of reasons, are beneficial to the enhancement of Seebeck coefficient. The lattice parameters are refined by Rietveld refinement of XRD data (Fig. 2Sb). The cell volume increases with increasing total doping concentration in the co-doped samples (Table S1). To clarify the reason for large Seebeck coefficient, we estimated the carrier effective mass using the following equations [17]:

$$m^* = \frac{h^2}{2k_BT}\left[\frac{n}{4\pi F_{\frac{1}{2}}(\xi)}\right]^{\frac{2}{3}} \quad (1)$$

$$F_r(\xi) = \int_0^\infty \frac{x^r}{1+e^{x-r}}dx \quad (2)$$

$$S = -\frac{K_B}{e}\left[\frac{(r+2)4\pi F_{r+1}(\xi)}{(r+1)4\pi F_r(\xi)} - \xi\right] \quad (3)$$

Where h, k_B,T, F_r, r and ξ are the Planck constant, Boltzmann constant, absolute temperature, Fermi integral, scattering parameter and chemical potential, respectively. The obtained m^*/m_0 values are listed in Table 1.

The critical concentration of degenerate $SrTiO_3$ semiconductor can be determined by following equation [31]:

$$a_H n_c^{1/3} = 0.26 \quad (4)$$

where a_H, n_c are the Bohr radius and critical concentration of degeneration. From the equation, n_c=7.95×10^{10} cm^{-3}, as for the present samples, the carrier concentration (> 10^{20} cm^{-3}) are far larger than the critical value. Therefore, S can be explained by the model proposed for degenerate semiconductors [32]:

$$S = \frac{8\pi^2k_B^2}{3eh^2}m^*T\left(\frac{\pi}{3n}\right)^{\frac{2}{3}} \quad (5)$$

where, k_B is Boltzmann constant, e is electronic charge, and n is the electron concentration of a doped semiconductor. It is seen that the S

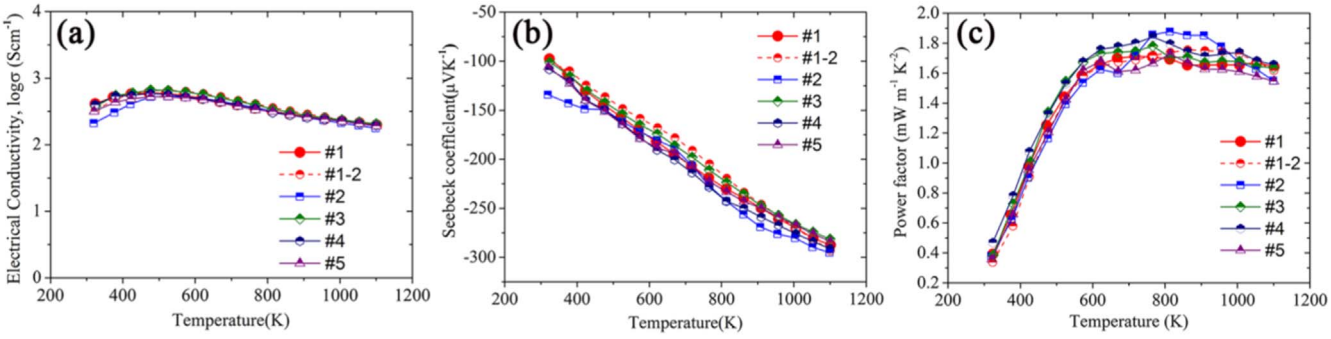

Fig. 4. Temperature dependent of (a) electrical conductivity (σ), (b) Seebeck coefficient (S), (c) power factor (PF) in the same La10Nb10 sample (#1 and #1–2) and different four La10Nb10 samples (#2-#5).

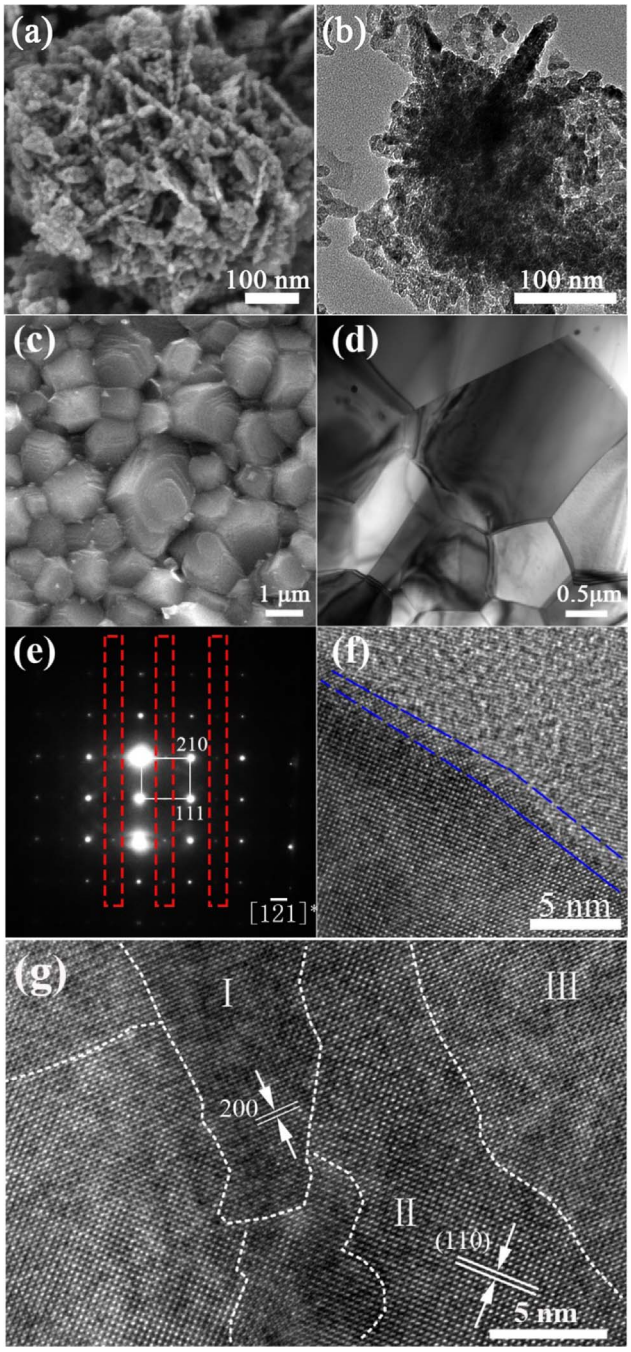

Fig. 5. SEM and TEM analyses of 10 mol% Nb-10 mol% La doped $SrTiO_3$ sample. (a) SEM and (b) TEM image of powder sample. (c) SEM and (d) TEM image of bulk sample. (e) Electron diffraction pattern of the large dark grain in (d). (f) HRTEM images of $SrTiO_3$ grain boundary. (g) HRTEM images in a grain of $SrTiO_3$.

values closely relate to $m^*/m_0n^{2/3}$ values. On the other hand, the high electrical properties depend primarily on large weighed mobility $\mu(m^*/m_0)^{3/2}$ [33]. The $m^*/m_0n^{2/3}$ and weighed mobility for the present samples are also listed in Table 1. Accordingly, the increase of *PF* in La10Nb10 sample could arise from optimized $m^*/m_0n^{2/3}$ and $\mu(m^*/m_0)^{3/2}$, which have been attributed to the modification of doping concentration and dopants type [34]. Therefore, the combination of large σ and high $|S|$ achieved by optimized doping concentration results in the large *PF* at high temperatures (Fig. 2d).

The temperature dependences of *PF*s between 300 K and 1100 K are shown in Fig. 2d. Although the *PF*s obtained in this study are not as high as the one observed in $Sr_{1-x}La_xTiO_3$ single crystals [30] nor the predicted theoretical calculation [35], the high values of 1.65–1.7 mW m^{-1} K^{-2} for the La10Nb10 sample are almost temperature independent in the range between 623 and 1100 K. Such a high *PF* value is among the top level in polycrystalline $SrTiO_3$ bulks. To confirm the stability of the electrical transport properties, one sample has been measured for more than two times and the repeatability of this property also has been confirmed in other four samples. The σ, $|S|$ and *PF* values of La10Nb10 sample are reproduced in many samples (Fig. 4) and the hall carrier concentration and mobility show no significant difference between the heating and cooling curves (Fig. S3), indicating the samples are stable at maximum measured temperature.

3.2. Thermal transport properties

The total thermal conductivity (κ_{total}) and lattice thermal conductivity (κ_L) of the various samples are shown in Fig. 2e-f, respectively. Nb and La co-doped samples have lower κ_{total} compared with that of Nb or La single-doped samples and the results reported previously [16]. The highest κ_{total} (4.58 W m^{-1} K^{-1}) in co-doped samples is observed in La5Nb5 sample at room temperature, which changes to the smallest value in all samples above 850 K, and monotonically decreases to ~2.59 W m^{-1} K^{-1} at 1100 K (Fig. 2d). In contrast, the La10Nb20 sample shows the lowest κ_{total} (3.73 W m^{-1} K^{-1}) at room temperature, which turns to be the highest value in co-doped samples above 850 K. This occurrence can be explained by temperature dependences of electronic thermal conductivity κ_e ($\kappa_e = LT\sigma$, where L is the Lorenz number of 2.44×10^{-8} V^2 K^{-2}) and κ_L, which is estimated by equation $\kappa_e = \kappa_{total} - \kappa_L$. The κ_e of all samples shows similar temperature dependence with σ, and increases with the increase of doping concentration at high temperatures above 650 K (Fig. S4). The κ_L shows contrary temperature dependence with κ_e in the same temperature range. At room temperature, the κ_L, which plays a dominant role in κ_{total}, decreases with increasing doping concentration. Such a decrement may be arisen from the additional phonon scattering that is due to the presence of impurities, defects, grain boundaries, etc. [3,36,37]. The phenomenon is remarkable in the La10Nb20 sample. Except for the La10Nb20, the κ_L deceases with the increasing temperature, indicating a dominant phonon scattering by the Umklapp process [34,38]. In addition, the contribution of difference of κ_e on κ_{total} becomes more prominent than difference of κ_L on κ_{total} in co-doped samples at high temperatures expect for La5Nb5 sample. In La5Nb5 sample, the contribution of κ_L to κ_{total} is dominated. The κ_L values of La5Nb5 sample are smaller than that of two single-doped samples at high temperature (850–1000 K), although they are similar at low temperature. The κ_L values of other co-doped samples with heavy doping concentration (> 10 mol%) are slightly smaller than single-doped samples in all temperature range, which is presumably due to the increase of lattice randomness by dopant [30].

3.3. Microstructures

To confirm the contributions of La and Nb doped nano-powders and sintering process on microstructure, which further modulate electronic and thermal transport properties, we carried out the analysis by SEM and TEM. Fig. 5a-b show the SEM and TEM images of La10Nb10 powder sample, respectively. It is well known that the size and quality of starting powders are important to achieve high thermoelectric performance [4]. In this study, nanoparticles with an average size of about 15 nm of La-Nb co-doped $SrTiO_3$ single phase (Fig. S2a) are obtained by employing the hydrothermal synthesis process, which provides a good foundation for the improvement of *ZT*. Except for the main phase of $SrTiO_3$, the TiO_2 second phases are precipitated during the sintering process (Fig. S2b). Fig. 5c shows the SEM image of bulk samples. Grains of 1–5 μm in size are sintered together and clear growth steps on the surfaces of grains are observed, indicating that the

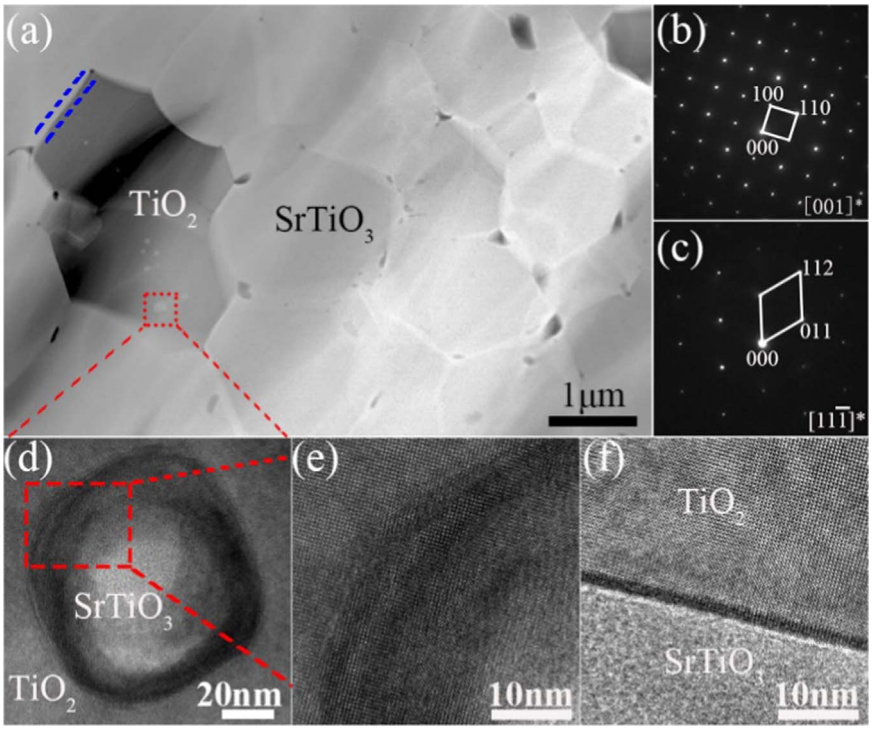

Fig. 6. STEM and HRTEM analyses of the La10Nb10 bulk sample. (a) STEM image of $SrTiO_3$ containing some TiO_2 grains (dark). (b) Electron diffraction pattern of TiO_2 grain and (c) Nano-inclusions of $SrTiO_3$ in TiO_2 grain. (d) HRTEM images of $SrTiO_3$ nano-inclusion and (e) enlarged interface of TiO_2 and $SrTiO_3$ nano-inclusion. (f) HRTEM image on grain boundary of $SrTiO_3$ and TiO_2 marked with blue lines in (a).

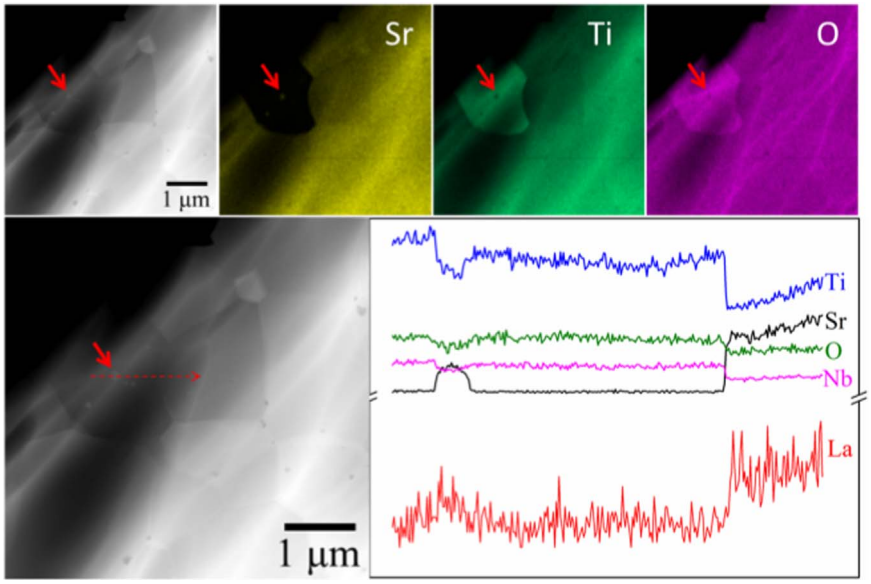

Fig. 7. TEM-EDS mapping on TiO_2 grain containing $SrTiO_3$ nano-inclusion and line-scan analyses along with the red dashed arrow of the La10Nb10 bulk sample.

samples are sintered smoothly and the grains grow during the sintering process. Sharpness of grains and associated grain boundaries are clearly evident in dark-field TEM images of bulk samples (Fig. 5d). Fig. 5e shows the election diffraction pattern of the La10Nb10 bulk sample. The superstructure reflections observed between regular perovskite $SrTiO_3$ reflections may be related to lattice modulation that arises from different dopants (Nb and/or La). The superstructure reflections also observed in other co-doped samples, but not in single doped of bulk sample (Fig. S5), which can partially contribute to its low thermal conductivity [39]. HRTEM is performed to observe the microstructures of grains and associated grain boundaries in bulk sample (Fig. 5f-g). The grain boundaries are ~2 nm in thickness and the coherency strain that derives from the small lattice mismatch is observed in the $SrTiO_3$ grains.

The presence of TiO_2 in $SrTiO_3$ bulk sample (as observed in XRD, Fig. S2b) is verified again by the combination of STEM observation and electron diffraction pattern (Fig. 6a-b), which shows that the dark TiO_2 grains are surrounded by light $SrTiO_3$ grains. In the TiO_2 grain, interestingly, $SrTiO_3$ nano-grains with sizes ranging from a few nm to 100 nm are clearly seen (Fig. 6c-d and Fig. S6), consisting of heterostructure of $SrTiO_3$ nano-inclusion/TiO_2 grain (Fig. 6e) and micro-sized $SrTiO_3$/TiO_2 grain with thin grain boundary of ~2 nm (Fig. 6f). The second phase, nano-inclusion ($SrTiO_3$ in TiO_2) and heterostructure may have some contribution to the enhancement of

phonon scattering [3,20,21] and energy filtering [8,40]. Although the trace precipitation of second phase results in the difference between nominal doping concentration and actual one, the ratio of Sr, La, Ti and Nb in La10Nb10 bulk sample obtained from energy dispersive spectrometers (EDS) attached with SEM (Fig. S7) and TEM (Fig. S8) are Sr: La: Ti: Nb =1: 0.14: 1.2: 0.15 and Sr: La: Ti: Nb =1: 0.13: 0.9: 0.14 respectively, which are close to the nominal one. Ratios of Sr, La, Ti and Nb in other samples are listed in Table S1. TEM-EDS mapping and line-scan (Fig. 7) in La10Nb10 bulk sample also show that the TiO_2 second phase, surrounded by $SrTiO_3$ grains, contains $SrTiO_3$ nano-inclusions, which is also observed in SEM-EDS mapping images (Fig. S9). One can see that each element homogenously distributed in the matrix of $SrTiO_3$ grains (Fig. 7). Ti and O are obviously brighter in TiO_2 grain when compared with $SrTiO_3$ because the ratio of Ti and O in TiO_2 is larger than that of $SrTiO_3$. Nb element is also observed in TiO_2 grains, indicating that the TiO_2 is doped by Nb. On the other hand, the ratios of Sr, Ti, Nb and O elements show a clearly difference in $TiO_2/SrTiO_3$ heterostructure. Although the precipitations of TiO_2 may induce the difference between nominal doping and actual doping concentration and the decreasing of σ [27], the high doping concentration can compensate these losses by increasing the carrier concentration (n). Meanwhile, the heavy doping of La^{3+} cation in A-site and Nb^{5+} cation in B-site can introduce the large lattice distortion as mentioned in TEM result and cell volume, which may also partially contribute to the reduction of thermal conductivity. A detailed study of the correlation between microstructure and thermoelectric properties will be the focus on the future work. A comprehensive understanding of the mechanism and microstructure controlling of co-doped $SrTiO_3$ requires further study in the near future, which may be the key to obtain more high $ZT > 1$.

4. Conclusions

The combination of hydrothermal method and high effective sintering successfully produced a nano-scale modulation doping in La-Nb-doped $SrTiO_3$ bulks. Nano-scale modulation doping achieved in this study has the triple functions: 1) La and Nb co-doping increases the carrier concentrations and electrical conductivity; 2) the Seebeck coefficients are enhanced by optimized $m^*/m_0 n^{2/3}$ and $\mu(m^*/m_0)^{3/2}$, which can be attributed to the modification of doping concentration and dopants type; 3) The thermal conductivity is reduced through complex microstructures, e.g., atomic-scale La and Nb doped effects, superlattice, TiO_2 second phases and nano-scale $SiTiO_3$ precipitates. Upon optimizing of electrical transport properties and reducing thermal conductivity by modification of dopants type and ratio, the thermoelectric performance can be significantly enhanced. A record high $ZT > 0.6$ at 1000 ~1100 K was achieved in La10Nb10 co-doped $SrTiO_3$ bulks. The nano-scale modulation doping and microstructure controlling approach pave the way to achieve further potential application on thermoelectric materials.

Acknowledgements

The authors are grateful to Prof. Yanzhong Pei at Tongji University for Hall measurements. This work supported by State Key Laboratory of New Ceramic and Fine Processing (Tsinghua University) under the No. KF201608, Guangxi Key Laboratory of Information Materials, Guilin University of Electronic Technology under the No. 151004-K. Natural Science Foundation of Inner Mongolia under the No. 2016BS0507 and 2015MS0530, National Natural Science Foundation of China under the Nos. 51525401, 51401044 and 51502147. This work was also partly supported by NSFC under Grant No. 51571007.

Appendix A. Supporting information

Supplementary data associated with this article can be found in the online version at doi:10.1016/j.nanoen.2017.04.003.

References

[1] L.D. Zhao, S.H. Lo, Y. Zhang, H. Sun, G. Tan, C. Uher, C. Wolverton, V.P. Dravid, M.G. Kanatzidis, Ultralow thermal conductivity and high thermoelectric figure of merit in SnSe crystals, Nature 508 (2014) 373–377.
[2] L.-D. Zhao, G. Tan, S. Hao, J. He, Y. Pei, H. Chi, H. Wang, S. Gong, H. Xu, V.P. Dravid, C. Uher, G.J. Snyder, C. Wolverton, M.G. Kanatzidis, Ultrahigh power factor and thermoelectric performance in hole-doped single-crystal SnSe, Science 351 (2016) 141–144.
[3] K. Biswas, J. He, I.D. Blum, C.I. Wu, T.P. Hogan, D.N. Seidman, V.P. Dravid, M.G. Kanatzidis, High-performance bulk thermoelectrics with all-scale hierarchical architectures, Nature 489 (2012) 414–418.
[4] B. Poudel, Q. Hao, Y. Ma, Y.C. Lan, A. Minnich, B. Yu, X.A. Yan, D.Z. Wang, A. Muto, D. Vashaee, X.Y. Chen, J.M. Liu, M.S. Dresselhaus, G. Chen, Z.F. Ren, High-thermoelectric performance of nanostructured bismuth antimony telluride bulk alloys, Science 320 (2008) 634–638.
[5] J. He, M.G. Kanatzidis, V.P. Dravid, High performance bulk thermoelectrics via a panoscopic approach, Mater. Today 16 (2013) 166–176.
[6] Y. He, P. Lu, X. Shi, F. Xu, T. Zhang, G.J. Snyder, C. Uher, L. Chen, Ultrahigh thermoelectric performance in mosaic crystals, Adv. Mater. 27 (2015) 3639–3644.
[7] H. Liu, X. Shi, F. Xu, L. Zhang, W. Zhang, L. Chen, Q. Li, C. Uher, T. Day, G.J. Snyder, Copper ion liquid-like thermoelectrics, Nat. Mater. 11 (2012) 422–425.
[8] C. Ou, J. Hou, T.-R. Wei, B. Jiang, S. Jiao, J.-F. Li, H. Zhu, High thermoelectric performance of all-oxide heterostructures with carrier double-barrier filtering effect, NPG Asia Mater. 7 (2015) e182.
[9] C. Wan, X. Gu, F. Dang, T. Itoh, Y. Wang, H. Sasaki, M. Kondo, K. Koga, K. Yabuki, G.J. Snyder, R. Yang, K. Koumoto, Flexible n-type thermoelectric materials by organic intercalation of layered transition metal dichalcogenide TiS_2, Nat. Mater. 14 (2015) 622–627.
[10] M. Ohtaki, K. Araki, K. Yamamoto, High thermoelectric performance of dually doped ZnO ceramics, J. Elec Mater. 38 (2009) 1234–1238.
[11] J. Lan, Y.-H. Lin, Y. Liu, S. Xu, C.-W. Nan, M. Hopper, High thermoelectric performance of nanostructured In_2O_3-based ceramics, J. Am. Ceram. Soc. 95 (2012) 2465–2469.
[12] Z. Lu, H. Zhang, W. Lei, D.C. Sinclair, I.M. Reaney, High-figure-of-merit thermoelectric La-doped A-site-deficient SrTiO3 ceramics, Chem. Mater. 28 (2016) 925–935.
[13] F. Ryoji, M. Ichiro, I. Hiroshi, T. Tsunehiro, M. Uichiro, S. Satoshi, An oxide single crystal with high thermoelectric performance in air, Jpn. J. Appl. Phys. 39 (2000) L1127.
[14] K. Fujita, T. Mochida, K. Nakamura, High-temperature thermoelectric properties of $Na_x CoO_{2-\delta}$ single crystals, Jpn. J. Appl. Phys. 40 (2001) 4644.
[15] H.P.R. Frederikse, W.R. Thurber, W.R. Hosler, Electronic transport in strontium titanate, Phys. Rev. 134 (1964) A442–A445.
[16] K. Park, J.S. Son, S.I. Woo, K. Shin, M.-W. Oh, S.-D. Park, T. Hyeon, Colloidal synthesis and thermoelectric properties of La-doped $SrTiO_3$ nanoparticles, J. Mater. Chem. A 2 (2014) 4217–4224.
[17] S. Ohta, T. Nomura, H. Ohta, M. Hirano, H. Hosono, K. Koumoto, Large thermoelectric performance of heavily Nb-doped $SrTiO_3$ epitaxial film at high temperature, Appl. Phys. Lett. 87 (2005) 092108.
[18] R.-Z. Zhang, C.-l. Wang, J.-c. Li, K. Koumoto, Simulation of thermoelectric performance of bulk SrTiO3 with two-dimensional electron gas grain boundaries, J. Am. Ceram. Soc. 93 (2010) 1677–1681.
[19] T. Teranishi, Y. Ishikawa, H. Hayashi, A. Kishimoto, M. Katayama, Y. Inada, X.D. Zhou, Thermoelectric efficiency of reduced $SrTiO_3$ ceramics modified with La and Nb, J. Am. Ceram. Soc. 96 (2013) 2852–2856.
[20] N. Wang, H. He, Y. Ba, C. Wan, K. Koumoto, Thermoelectric properties of Nb-doped $SrTiO_3$ ceramics enhanced by potassium titanate nanowires addition, J. Ceram. Soc. Jpn. 118 (2010) 1098–1101.
[21] N. Wang, H. Chen, H. He, W. Norimatsu, M. Kusunoki, K. Koumoto, Enhanced thermoelectric performance of Nb-doped $SrTiO_3$ by nano-inclusion with low thermal conductivity, Sci. Rep. 3 (2013) 3449.
[22] A. Kikuchi, N. Okinaka, T. Akiyama, A large thermoelectric figure of merit of La-doped $SrTiO_3$ prepared by combustion synthesis with post-spark plasma sintering, Scr. Mater. 63 (2010) 407–410.
[23] B.R. Sudireddy, K. Agersted, Sintering and electrical characterization of La and Nb co-doped $SrTiO_3$ electrode materials for solid oxide cell applications, Fuel Cells 14 (2014) 961–965.
[24] H. Ohta, S. Kim, Y. Mune, T. Mizoguchi, K. Nomura, S. Ohta, T. Nomura, Y. Nakanishi, Y. Ikuhara, M. Hirano, H. Hosono, K. Koumoto, Giant thermoelectric Seebeck coefficient of a two-dimensional electron gas in $SrTiO_3$, Nat. Mater. 6 (2007) 129–134.
[25] Y. Wang, F. Li, L. Xu, Y. Sui, X. Wang, W. Su, X. Liu, Large thermal conductivity reduction induced by La/O vacancies in the thermoelectric $LaCoO_3$ system, Inorg. Chem. 50 (2011) 4412–4416.
[26] A.V. Kovalevsky, A.A. Yaremchenko, S. Populoh, A. Weidenkaff, J.R. Frade, Effect of A-site cation deficiency on the thermoelectric performance of donor-substituted strontium titanate, J. Phys. Chem. C 118 (2014) 4596–4606.
[27] B. Zhang, J. Wang, T. Zou, S. Zhang, X. Yaer, N. Ding, C. Liu, L. Miao, Y. Li, Y. Wu, High thermoelectric performance of Nb-doped $SrTiO_3$ bulk materials with different doping levels, J. Mater. Chem. C 3 (2015) 11406–11411.
[28] J. Shen, X. Zhang, S. Lin, J. Li, Z. Chen, W. Li, Y. Pei, Vacancy scattering for enhancing the thermoelectric performance of CuGaTe2solid solutions, J. Mater. Chem. A 4 (2016) 15464–15470.

[29] J. Sun, D.J. Singh, Thermoelectric properties of n-type $SrTiO_3$, APL Mater. 4 (2016) 104803.
[30] T. Okuda, K. Nakanishi, S. Miyasaka, Y. Tokura, Large thermoelectric response of metallic perovskites: $Sr_{1-x}La_xTiO_3$ (0≤ x≤0.1), Phys. Rev. B 63 (2001) 113104.
[31] P.P. Edwards, M.J. Sienko, Universality aspects of the metal-nonmetal transition in condensed media, Phys. Rev. B 17 (1978) 2575–2581.
[32] M. Cutler, J.F. Leavy, R.L. Fitzpatrick, Electronic transport in semimetallic cerium sulfide, Phys. Rev. 133 (1964) A1143–A1152.
[33] Y. Pei, A.D. LaLonde, H. Wang, G.J. Snyder, Low effective mass leading to high thermoelectric performance, Energy Environ. Sci. 5 (2012) 7963.
[34] S. Ohta, T. Nomura, H. Ohta, K. Koumoto, High-temperature carrier transport and thermoelectric properties of heavily La- or Nb-doped $SrTiO_3$ single crystals, J. Appl. Phys. 97 (2005) 034106.
[35] K. Shirai, K. Yamanaka, Mechanism behind the high thermoelectric power factor of SrTiO3 by calculating the transport coefficients, J. Appl. Phys. 113 (2013) 053705.
[36] B. Qiu, H. Bao, G. Zhang, Y. Wu, X. Ruan, Molecular dynamics simulations of lattice thermal conductivity and spectral phonon mean free path of PbTe: bulk and nanostructures, Comput. Mater. Sci. 53 (2012) 278–285.
[37] Y. Wang, K. Fujinami, R. Zhang, C. Wan, N. Wang, Y. Ba, K. Koumoto, Interfacial thermal resistance and thermal conductivity in nanograined $SrTiO_3$, Appl. Phys. Express 3 (2010) 031101.
[38] W. Li, S. Lin, X. Zhang, Z. Chen, X. Xu, Y. Pei, Thermoelectric properties of Cu_2SnSe_4 with intrinsic vacancy, Chem. Mater. 28 (2016) 6227–6232.
[39] Y. Wang, K.H. Lee, H. Ohta, K. Koumoto, Thermoelectric properties of electron doped $SrO(SrTiO_3)n$ (n=1,2) ceramics, J. Appl. Phys. 105 (2009) 103701.
[40] Y. Wang, X. Zhang, L. Shen, N. Bao, C. Wan, N.-H. Park, K. Koumoto, A. Gupta, Nb-doped grain boundary induced thermoelectric power factor enhancement in La-doped $SrTiO_3$ nanoceramics, J. Power Sources 241 (2013) 255–258.

Jun Wang is an Associate Professor of School of Materials Science and Engineering at Inner Mongolia University of Technology. He received his B.E. degrees in Physics Science from the Inner Mongolia Normal University, M.E. degrees under supervision of Prof. Masaya Ichimura and Ph.D. degree under supervision of Prof. Nobuo Ishizawa in Materials Science from the Nagoya Institute of Technology, Japan in 2011. His research interests include the thermoelectric materials, oxide semiconductor and wear resistant materials.

Bo-Yu Zhang received his Master's Degree in 2016 from School of Materials Science and Engineering, Inner Mongolia University of Technology, Inner Mongolia, China. His research mainly focuses on the $SrTiO_3$ based thermoelectric materials.

Hui-Jun Kang is an Associate Professor of Materials Science and Engineering at Dalian University of Technology, China. He received his B.E.(2006), M.E. (2009) and Ph.D. (2013) degrees under the supervision of Prof. Jing-Jie Guo in Materials Science and Engineering from the Harbin Institute of Technology, China. He was a postdoctoral research fellow with Prof. Tong-Min Wang in Materials Science and Engineering at Dalian University of Technology from 2013 to 2015. His research interests include the solidification, metal matrix composite, in situ visualization by synchrotron microradiography and thermoelectric materials.

Yan Li is Master degree candidate of Materials Science and Engineering, Inner Mongolia University of Technology, Inner Mongolia, China. Her research mainly focuses on the $SrTiO_3$ based thermoelectric materials.

Xinba Yaer is an Associate Professor of School of Materials Science and Engineering at Inner Mongolia University of Technology. He received his B.E. degrees in foundry process and M.E. degrees under supervision of Prof. Bao Yin from Inner Mongolia University of Technology, China in 2002. And then he received his Ph.D. degree under supervision of Prof. Kazumichi Shimizu in Materials Science from Muroran Institute of Technology, Japan in 2007. His research interests include wear resistant materials and the thermoelectric materials.

Jing-Feng Li is a “Changjiang Scholar” distinguished professor of Materials Science and Engineering, Tsinghua University. He graduated in 1984 from the Huazhong University of Science and Technology, China, and received master and doctor degrees both from Tohoku University, Japan. Before joining Tsinghua University as a full professor in 2002, he worked in Tohoku University as an assistant professor (1992–1997) and an associate professor (1997–2002). His research group focuses on thermoelectric and piezoelectric materials as well as their micro fabrication technology.

Qing Tan received a Ph.D. degree in July 2016 in the School of Materials Science and Engineering, Tsinghua University, Beijing, China. She received a B.E. degree in Materials Science and Engineering from Tsinghua University in 2011. After the B.E. study, she joined Prof. Jing-Feng Li's group in the State Key Laboratory of New Ceramics and Fine Processing in Tsinghua University. Her recent research focused on Sn-S based thermoelectric materials.

Shuai Zhang is an Associate Researcher of Institute of Physics Chinese Academy of Sciences. He received his B.E. degree in Physics Science from Henan Normal University. He received his master and doctor degree in Physics Science from Toyama University in Japan. He finished his postdoctoral researches at Hiroshima University in Japan, and Kent State University in USA. His research interests include heavy fermion, magnetic compound, strongly correlated electron system and superconductor materials.

Guo-Hua Fan is an Associate Professor of Materials Science and Engineering at Harbin Institute of Technology, China. He received his B.E. in Materials Science from the China University of Mining and Technology and his Ph.D. degree under the supervision of Prof. Lin Geng in Materials Science from Harbin Institute of Technology, China in 2009. His research interests include the design, fabrication and advanced characterization of metal and composites.

Cheng-Yan Liu is an Assistant Professor of School of Material Science and Engineering, Guilin University of Electronic Technology. He received his B.E. degree in chemical engineering and technology from Taiyuan University of Science and Technology. He received his master and doctor degree from University of Chinese Academy of Sciences in 2013. He was appointed as an assistant researcher GuangZhou Institute of Energy Conversion, Chinese Academy of Sciences during 2013–2015. His research interests include preparation and thermoelectric mechanism study of layered selenide bulk materials.

Lei Miao received a Ph.D. degree from Nagoya Institute of Technology (NITtech.), Japan. She became a professor in Guilin University of Electronic Technology after she worked in Guangzhou Institute of Energy Conversion, Chinese Academy of Sciences (CAS), where he was awarded CAS 100 talent program. Dr. Miao won Science and Technology Award of Guangxi Provence of 2016, Guangdong Provence of 2013. She was ever appointed as a research associate professor in NITtech., a deputy research leader in Japan Fine Ceramics Centre during 2004-2008. Her current research focuses on synthesis, mechanism and application of energy conversion materials.

Ding Nan is an assistant professor of Inner Mongolia University of Technology. He received a PhD in Materials Science and Engineering from Tsinghua University (China) in 2014. His current research focus is on the Carbon nanomaterials and their application in high-efficient energy storage systems such as flexible lithium-ion batteries, lithium–sulfur batteries, sodium-ion batteries, supercapacitors, etc.

Tong-Min Wang is a professor at Dalian University of Technology, China. He has obtained 'The National Science Fund for Distinguished Young Scholars" and "Yangtse Rive Scholar Bonus Schemes" of China. He received his B.E. and M.E. degrees under the supervision of Prof. Jing-Jie Guo in Harbin Institute of Technology and Ph.D. degree under Prof. Jun-Ze Jin in Dalian University of Technology, China in 2000. He was a postdoctoral research fellow with Prof. Itsuo Ohnaka and continued a fellow with Prof. Andreas Ludwig from 2000 to 2005. His research interests include the non-ferrous alloys, thermoelectric materials, metal-matrix composite and high-entropy alloys.

Li-Dong Zhao is a full Professor of Materials Science and Engineering at Beihang University, China. He received his B.E. and M.E. degrees in Materials Science from Liaoning Technical University and his Ph.D. degree in Materials Science from University of Science and Technology Beijing, China, in 2009. He was a postdoctoral research fellow in the ICMMO at University of Paris-Sud from 2009 to 2011 and continued as a postdoctoral research fellow in the Department of Chemistry at Northwestern University from 2011 to 2014. His research interests include the fabrication and characterizations of layered structural thermoelectrics, superconductors, and thermal barrier coatings.